IOSR Journal of Applied Chemistry (IOSR-JAC)
e-ISSN: 2278-5736. Volume 17, Issue 11 Ser. 1 (November 2024), PP 24-35
www.iosrjournals.org

Augmentation Of The Supercapacitive Performance Of Mn_3O_4 Nanoparticles By Doping Ni.

R. Mallikarjuna Sharma, M. Deepak, B. Haritha, V. Guru Prasad, O.M.Hussain
Department Of Physics, SVU College, Sri Venkateswara University, Tirupati, India.

Abstract:
Ni-doped Mn_3O_4 nanoparticles (NMO) with a morphology facilitating high surface area were synthesized by prudent hydrothermal synthesis, manifesting a supercapacitive tone with high specific capacitance and excelling cyclability. NMO nanoparticles were agglomerated from hydrated manganese chloride, hydrated nickel chloride, and sodium hydroxide precursors. The XRD results demonstrated predominant peaks oriented from (211), analogous to the I41/amd space group tetragonal structure. The Raman studies affirmed the bonding characteristics of vibration and bending modes of the Mn-O bond. The SEM inquiries proclaimed the morphology providing a large surface area. EDAX reports infer the elemental composition for phase purity confirmation of elements Mn, O, and Ni. Electrochemical accusation exhibited a pseudocapacitive character through cyclic voltammetry. The GCD deductions evince a specific capacitance of 565 F/g for Mn_3O_4 electrodes and 626 F/g for 0.6% NMO electrodes at a specific current of 0.5 A/g. These NMO electrodes achieved a cyclic capacitance rate of 82% after 3600 cycles.

Key Words*: Hydrothermal synthesis, Ni:Mn_3O_4 nanoparticles and specific capacitance.*

Date of Submission: 03-11-2024 Date of Acceptance: 13-11-2024

I. Introduction

The world lay claim to the burgeoning of electrochemical storage devices for copious storage of electrical energy [1-3]. Stereotype of devices are supercapacitors. Supercapacitors (SC) or ensorcelled electrochemical capacitors, have array of applications in electric, electronic and communications widgets [4]. In low-energy-density and high-power-density applications, batteries surrogate SCs [5-8]. Pseudocapacitive materials boast fast surface redox reactions and encompass high specific capacitance [9, 10]. Research is forged ahead to procure high specific capacitance from materials with pseudocapacitive properties from transition metal oxides like RuO_2 [11], Co_3O_4 [12], NiO [13], CuO [14], SnO_2 and Manganese oxides [15]. The study explores the application of Mn_3O_4 nanoparticles as electrodes for a supercapacitor to enhance its specific capacitance, highlighting the potential of the material when a transitional element is added to its composition [16, 17]. The material was chosen due to its high theoretical specific capacitance 1370 F/g [18], effective Jahn-Teller effect [18], wide potential window, variable oxidation states, environmental friendliness, non-toxicity, and cost-effectiveness [19, 20]. The survey indicates that the specific capacitance can reach up to 832 F/g [21] under different current densities and scan rates for thin films while it can reach 435 F/g at 1mV/s scan rate by hydrothermal method [22]. The study put in place that Ni-Al double-layered hydroxides had a specific capacitance value of 795 F/g at 1A/g, indicating good charge/discharge stability in solvothermal route [23]. To increase the specific capacitance of Mn_3O_4 through hydrothermal method, transition element Nickel was doped at different concentrations of 0.3%, 0.6% and 0.9%. This work focuses on the electrochemical properties of Ni doped Mn_3O_4 particles by hydrothermal way. Ni was chosen, due to its 0.72Å ionic radius, a close proximity to Mn's ionic radius of 0.80 Å, [24] resulting in minimal distortion in the structure and minimizing Jahn-Teller effect. The work explores and refines the electrochemical properties of the doped material, for its outwitting specific capacitance of 626 F/g at a specific current of 0.5 A/g for 0.6% Ni doped Mn_3O_4.

II. Experimental Procedure

First Mn_3O_4 nanoparticles lay the ground work and are characterized for elemental, microstructural, morphological and electrochemical properties. Then, Ni doped manganese oxide, Ni:Mn_3O_4 nanoparticles were synthesized for the betterment of electrochemical properties.

***Hydrothermal synthesis*:** Hydrated Manganese Chloride ($MnCl_2.4H_2O$) and Sodium Hydroxide (NaOH) procured from Merck co., were taken as precursors [25]. 1M $MnCl_2.4H_2O$ was primed by dissolving 4.95g of it, in 25ml of double distilled (DD) water in a 100ml beaker. 25ml of DD water was taken in a 50ml beaker and

1.0g of NaOH was dissolved in it for the composition of 1M NaOH solution. After the two solutes were completely dissolved, 100ml beaker containing Manganese Chloride was taken on the pan of a magnetic stirrer and was kept under stirring. Now, NaOH solution was added to Mn_3O_4 solution at a snail's pace by drop wise, stirring Mn_3O_4 solution continuously. Now the resultant liquid was transferred to Teflon lined autoclave. The autoclave was kept in a furnace and was heated for 6 hours at 450K. In this way the Mn_3O_4 nano particles were prepared at three reaction time periods of 6hrs, 10hrs and 14hrs respectively at a reaction temperature of 450K. After the furnace was cooled to room temperature, autoclave was brought out from the furnace and the liquid in it was slowly filtered with filter paper lined to a funnel. It was washed with DD water and ethanol for few times. The precipitate in the filter paper was dried beneath halogen lamp for one hour. Further, these precipitate particles were grinded for one hour with a mortar. The obtained dark brown particles were the nanoparticles of Mn_3O_4. To prepare 0.3%, 0.6% and 0.9% Ni doped Mn_3O_4 nanoparticles, 17mg, 34mg and 52mg of $NiCl_2.6H_2O$ were added respectively to 4.95g $MnCl_2.4H_2O$ in 25ml DD water.

***Material characterization*:** X-Ray Diffraction (XRD), Raman spectroscopy, Scanning Electron Microscopy (SEM) and Electrochemical analysis manoeuvred for characterization of Mn_3O_4 nanoparticles and Ni:Mn_3O_4 nanoparticles. Microstructure of the particles was delved by using X-ray diffractometer varying 2θ in the range of 10° to 70° as displayed in figure 1. The Raman spectrum for the prepared nanoparticles was inspected in the wave number range of 200 to 900cm^{-1}. Surface morphology was examined by scanning electron microscope. The elements unveiled in the nanoparticles were mounted from EDAX system. Electrochemical exploration was accomplished by composing electrodes from the prime powder, carbon black and polyvinylidene fluoride in 8:1:1 ratio. N-Methyl-2-Pyrrolidone (NMP) drops in few were added to the above grinded powder to make fine slurry. Chemically cleaned nickel strip substrate was brush coated with the slurry. NMP solvent was vaporized by heating to 480K. The prepared strip was working electrode in three electrode system for exploring Cyclic voltammetry (CV), Chronopotentiometry (CP) for galvanostatic charge discharge (GCD) studies and Electrochemical Impedance Spectrum (EIS) meant for the track down of specific capacitance.

III. Results And Discussion

Structural analysis:

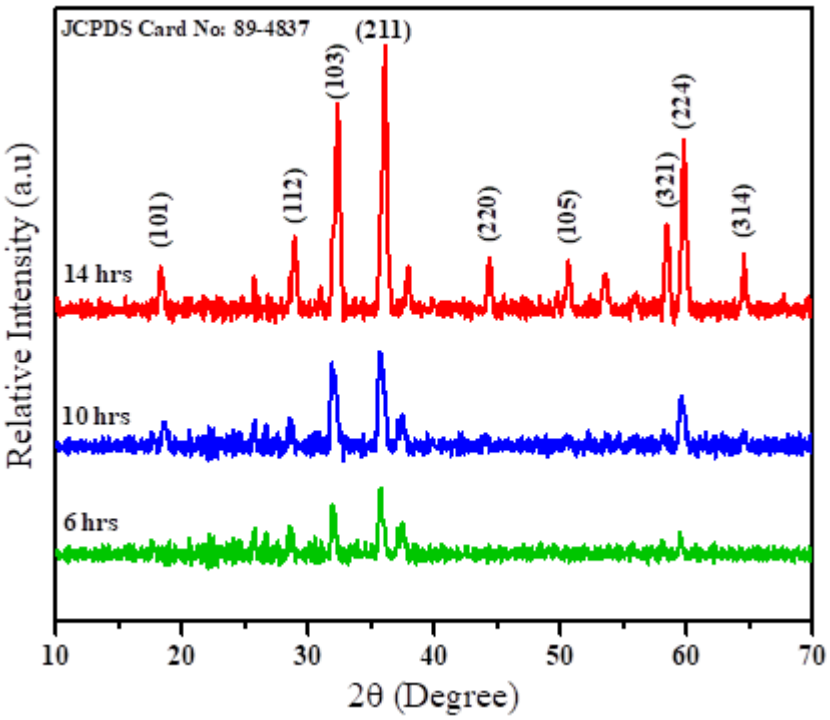

Fig. 1: XRD spectra of Mn_3O_4 nanoparticles synthesized at 6, 10, and 14 hours of reaction time periods at 450K temperature at 1M concentration of NaOH.

XRD studies: Fig. 1 uncovers XRD characteristics divulge by maximum diffraction peaks prop at 2θ values of 36.10°, 32.35°, 59.80°, 28.95°, 18.30°, 58.45°, 50.70°, 44.40° and 64.60°. They affirm the peak positions of JCPDS card no:89-4837 for Millar planes (211), (103), (224), (112), (101), (321), (105), (220) and (314) respectively. They promulgated I41/amd(141) space group owing to tetragonal structure for Mn_3O_4. It was in

consummation of the results obtained from the prior literatures reviewed [19]. From the primeval literature evaluation, reaction temperature was espoused at 450K. At 450K reaction temperature for the reaction time of 6 hours, the peaks designated to (211) and (103) rose to a little extent. At a reaction temperature of 450K, the reaction times were further increased to 10 and 14 hours. At a reaction time of 10 hours peaks consistent with (224) and (103) were also emerged along with heighten of antecedent peaks (211) and (103). When the reaction time was mounted up to 14 hours at the same temperature of 450K, particles manifest perpetual crystallinity with imperishable number of sharp peaks as put on display in fig. 1 and were borne for further processes. These optimal temperatures and time were in obedience to the quondam literatures of hydrothermal synthesis [26]. Lattice parameters evaluated from XRD data were a = b = 5.745Å and c = 9.346Å as witnessed in the Table no: 1. They were well harmonized with the standard JCPDS card no:89-4837. Parameters 'a' and 'b' were literal to graded values of JCPDS data, while 'c' deviated with a permittable percentage error 1.16.

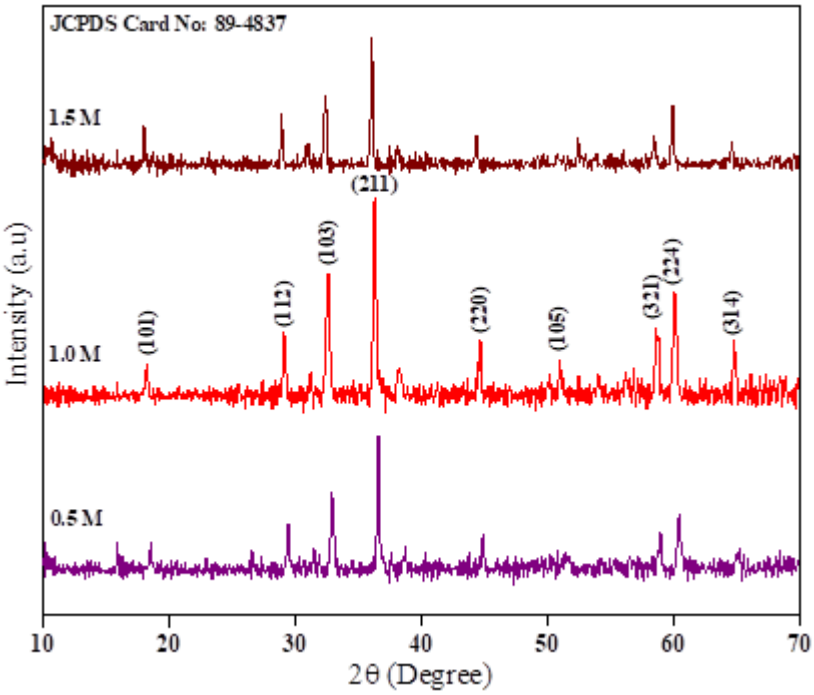

Fig. 2: XRD spectra of Mn_3O_4 nanoparticles synthesized with 0.5, 1.0 and 1.5M concentrations of NaOH at reaction temperature of 450K for 14 hours.

Table 1: Lattice parameters of Mn_3O_4 particles.

S.No	Lattice parameter	Calculated In Å	Standard In Å	% Error
1	a	5.745	5.763	0.3
2	b	5.745	5.763	0.3
3	c	9.346	9.456	1.16

The clout of variation of NaOH was also keenly detected. At 0.5M and 1.5M concentrations of NaOH, the spectral intensities were curtailed, indicating the best optimum concentration was 1M at locked reaction time of 14 hours at 450K. Also, with the increase of NaOH concentration, the characteristic peak (211) was slightly drifting towards lower values of 2θ, which was the general trend with the increase of oxidizing agent. 1M NaOH concentration along with 14 hours reaction time at 450K was used for the further prepared Ni doped Mn_3O_4 nanoparticles. The literature inspection, and the current experimental output have shown that Ni doping at the concentration levels taken up does not brought striking effect to the structure of Mn_3O_4 [27] as the ionic radii of Mn and Ni were close. At 0.6% of Ni doping, the doped atoms occupied tetrahedral Ni^{2+} ions occupied Mn^{2+} tetrahedral sties to a maximum extent without occupying the same sites besides them which increased void space between these sites.

Raman studies: In the course of coalescence of the particles, the stoichiometric ratio of NaOH was rooted by suss out Raman spectra of the contrived particles. The superior peak at 654.55 cm^{-1} devoted to stretching vibration symmetric mode A_{1g} of Mn^{2+} in Mn-O bond. The peak at 306.83 cm^{-1} was pertained to out of plane bending of E_{g2} symmetric mode. And the peak at 360.66 cm^{-1} was the sake of asymmetric stretch of bridge

oxygen structure Mn-O-Mn. With the hike of NaOH concentration from 0.5M to 1.5M through 1.0M, which was a precise stoichiometric ratio, the ascendant peak at 654 cm^{-1} mounted maximum intensity. Furthermore, the peaks at 306.83 and 360.66 cm^{-1} were also surge compared to other proportions of NaOH as shown in fig. 3. It was also chronic with XRD exploration. In XRD studies, slight drift of peaks was observed in fig. 2, which happens with the increase of oxidizing agent, NaOH.

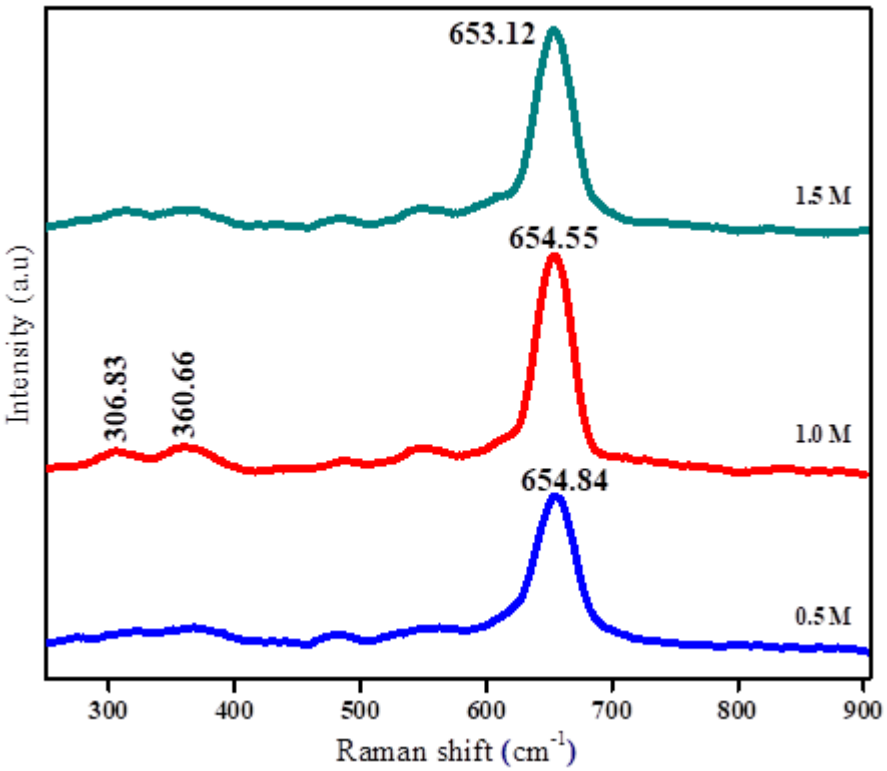

Fig. 3: Raman spectra of Mn_3O_4 particles synthesized at 450K for 14 hours, at 0.5, 1.0, and 1.5M NaOH concentrations.

The peaks at 307, 361cm^{-1} were meagre and 654cm^{-1} were low at reaction temperature of 450K for 14 hours for NaOH concentrations of 0.5M and 1.5M. For 1M NaOH concentration the characteristic peaks were more exhibitive indicating stoichiometric ratio at the same reaction temperature and time period as delineated in fig. 3. The doping of Ni atoms to the structure increased the stretching of M-O bonds both at tetrahedral and octahedral sites initially. When doping increases, with the occupancy of first tetrahedral sites, distortion occurred between the two tetrahedral sites. The distortion reduced when the doping was increased beyond 0.6%. Maximum stretching at this concentration created scope for the movement of ions for intercalation and deintercalation.

Morphological studies: To inquire the morphology of the particles, SEM exploration was taken up. Surface morphology of undoped and doped particles disseminates the particle morphology and was proliferating with the escalation of temperature. It was in concurrence with the results from literature consideration [28]. Figure 4 unfurl the SEM images (a), (b), (c) and (d), for pure Mn_3O_4 nanoparticles at reaction times of 6, 10, 14 hours and 0.6% Ni:Mn_3O_4 particles at 14 hours reaction time, all synthesized at 450K. The structure in (d) was with more particle size when compared to previous three. It for bye ensured compact with the prior proclaimed literature [22]. Image (d) pictured in figure 4, perspicuously opens the particle size was dominant at 0.6% Ni, in comparison to other three. Further, setting (d) side by side with (c), the particle size in (d) for 0.6% was affluence little than that of in (c). EDAX spectrum of the Mn_3O_4, elementary overlay and EDAX spectrum of 0.6% Ni:Mn_3O_4 particles visualization confirm the phase pure composition of the particles as set out in figures 5, 6 and 7 respectively.

IV. Experimental Procedure

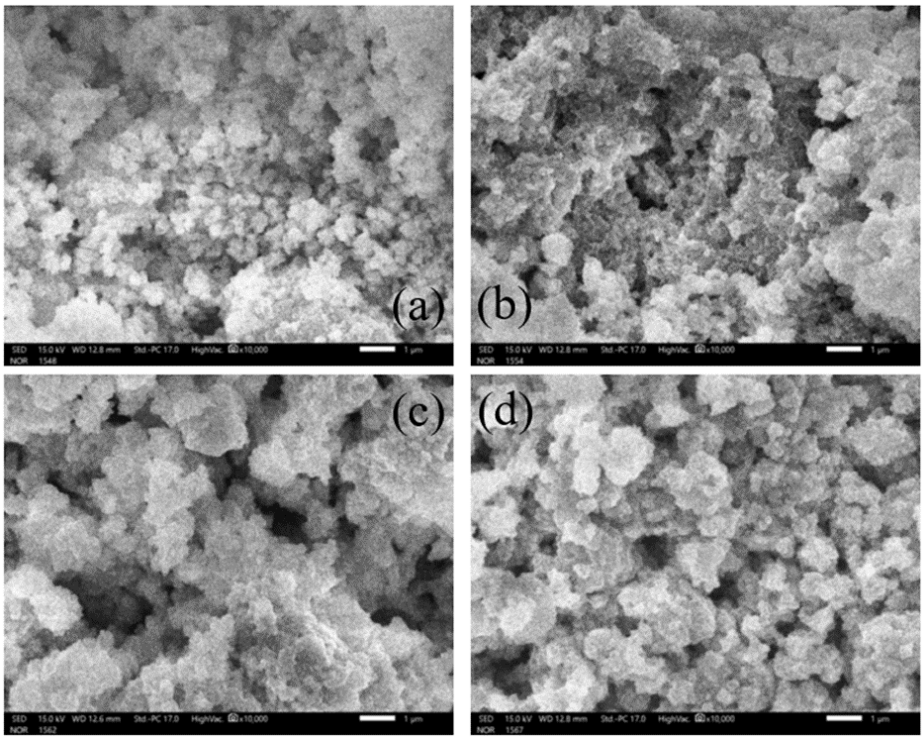

Fig. 4: SEM images of Mn_3O_4 synthesized at 450K using for (a) 6hrs, (b) 10hrs, (c) 14hrs and (d) 14hrs for Ni: Mn_3O_4 nanoparticles.

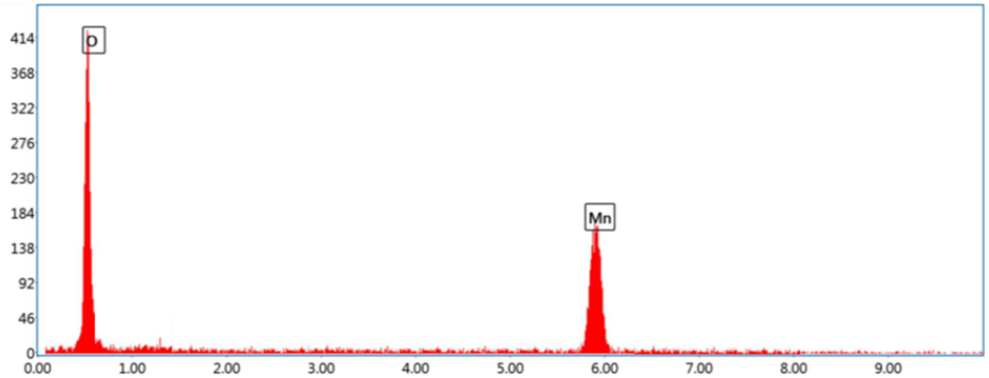

Fig. 5: EDAX spectrum for pure Mn_3O_4 nanoparticles synthesized at 450K for 14hours at 1M NaOH concentration.

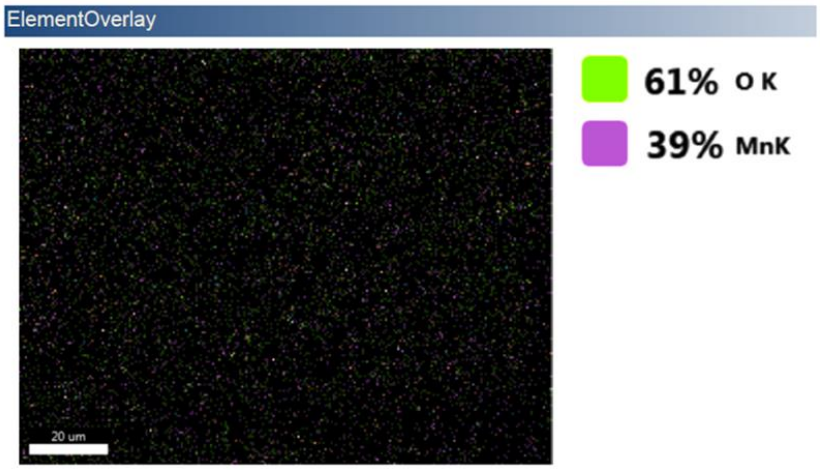

(a)

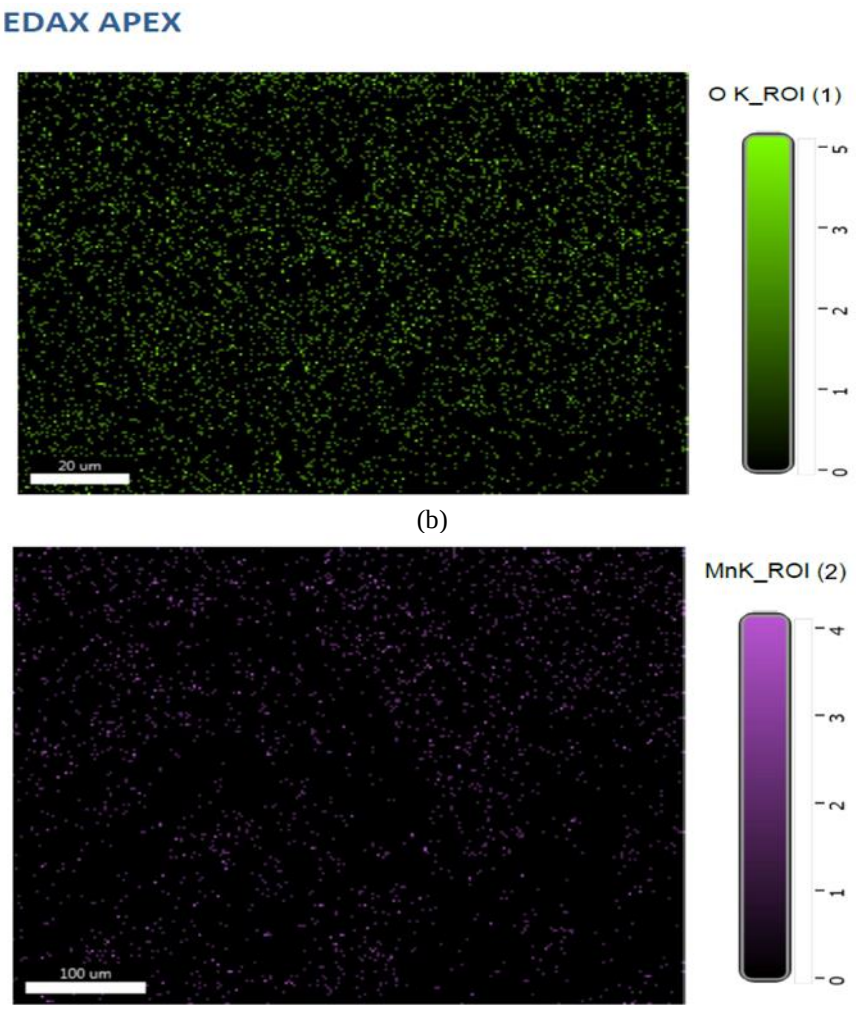

Fig. 6: EDAX images of Mn_3O_4 nanoparticles, (a) Elementary overlay, APEX images of element (b) Oxygen and (c) Manganese.

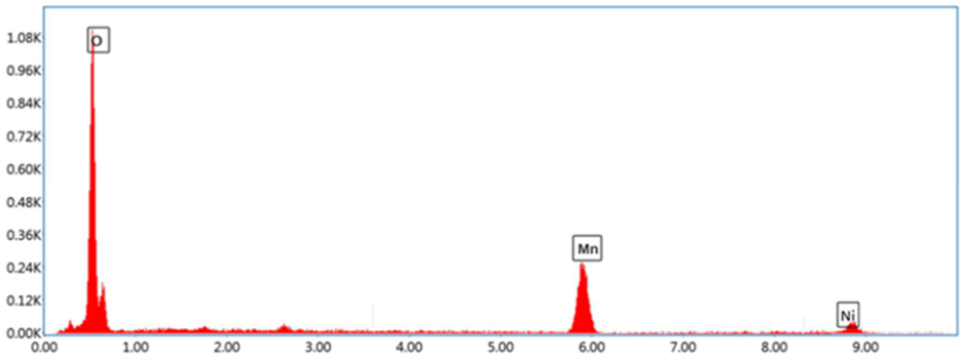

Fig. 7: EDAX spectrum for Mn_3O_4 nanoparticles doped with Ni at 0.6% concentration synthesized at 450K for 14 hours prepared at 1M NaOH concentration.

Electrochemical analysis: Working electrode was assembled from nanoparticulate sample powder, carbon black and Polyvinylidene fluoride (PVDF) quantified in the ratio 8:1:1, computed to 100 mg. Carbon black accomplish conduction while PVDF binds the particles. The pastiche was grinded for half an hour in a motor. Few drops of N-Methyl-2-Pyrrolidone (NMP) were added to it to make a fine homogeneous slurry. It was glazed on nickel plate with a brush, up to three quarters on one side. Owing the fact of 475 K boiling point for NMP, it was effaced by inflamed air in a furnace at 480K. Mn_3O_4 and Ni:Mn_3O_4 working electrodes were assembled by tightly encased copper wire to the other side of nickel plate and substrate was masked by Teflon

tape. CHI608C three-electrode electrochemical workstation was handled to explore the electrochemical properties of the electrodes.

Cyclic voltametric studies: Mn_3O_4 working electrode, Platinum disc counter electrode and Platinum foil reference electrode in 1M Na_2SO_4 electrolyte were maneuverer in a three-electrode electrochemical analyser. Super capacitive performance of the electrode material was evaluated from the CV curves inside the potential window of 1V, i.e., from -0.9V to 0.1V at scan rates of 3mV/s to 15mV/s in the steps of 3mV/s be seen in figure 7. $\frac{\int I(V)dV}{2\ m\ S_r P_w}$ expression was employed for the reckoning the specific capacitance (C_s) of the electrode material. Here $\frac{1}{2}\int I(V)\ dv$ is area enclosed by CV loop, m is active mass, S_r is scanning rate and P_w is potential window. C_s of Mn_3O_4 electrodes quantified at 315, 291, 268, 251 and 232 F/g at scan rates of 3, 6, 9, 12 and 15mV/s respectively and were put on show in table 2. These values were in line with previous literature values of hydrothermal process. In an idea to improvise them, another transition metal element in the form of nickel (Ni) was doped at various proportions. The doped Ni:Mn_3O_4 electrodes at 0.3%, 0.6% and 0.9% of Ni were trailed for the furtherance of C_s. The concerning C_s at the scan rate of 3 mV/s emanated for 0.3%, 0.6% and 0.9% Ni:Mn_3O_4 electrodes were 384, 421 and 396 F/g respectively. The C_s values were increased by 21.9%, 33.7% and 25.7% by doping Ni at the said proportions in series compared with pure Mn_3O_4 nanoparticles.

The augmentation in C_s values was ascribed to the increase in void space between side-by-side Mn^{2+} due to occupancy of one of it. changes in the ionic size and interaction between ions and electrons at the surface. Mn_3O_4 structure consists of tetrahedral and octahedral elements for Mn^{2+} and Mn^{3+} ions respectively. Mn^{2+} ions are bonded to four oxygen ions and Mn^{3+} ions by six oxygen ions. Also packing fractions for these elements were 0.78 and 0.72 [28, 29]. Considering these factors, at initial doping percentages, Ni ions easily occupy Mn^{2+} sites until packing fraction decreases to its minimum.

The area of the CV loop was decreasing with the decrease in the scan rate. It means that, as the scan rate decreases, charges were finding time for intercalation and deintercalation. The area enclosed by the loop decreases to bring an ideal rectangular situation where the increase and decrease of voltage and current are almost parallel to voltage and current axes respectively. The area of the CV loop was low at 0.6% Ni concentration. It was more at concentrations below and above that concentration for a scan rate of 3mV/s. At scan rate below 3mV/s, the cures were fluctuating because of low current densities.

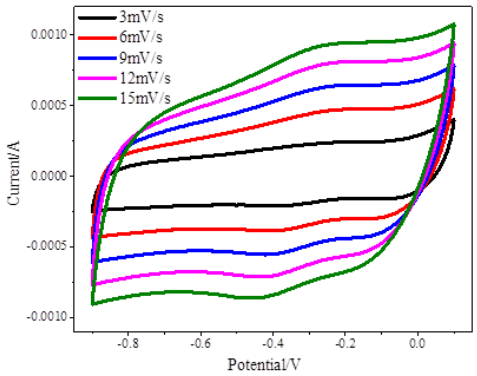

Fig. 8: CV curves of pure Mn_3O_4 electrodes synthesized at 450K for 14 hours at scan rates of 3, 6, 9, 12 and 15mV/s.

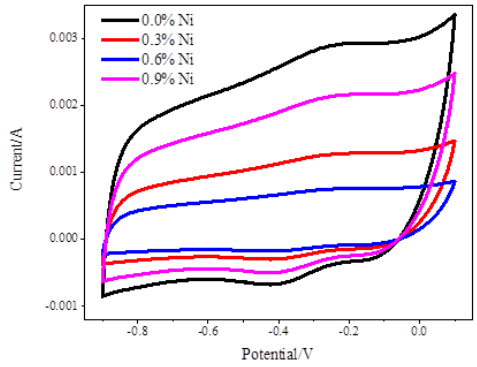

Fig. 9: CV curves of electrodes of pure Mn_3O_4 and Ni:Mn_3O_4 electrodes doped with 0.6% concentration of Ni synthesized at 450K for 14 hours at scan rate of 3mV/s.

Table 2: Cs values from CV curves of Mn3O4 electrodes.

S.No	Scan Rate in mV/s	Specific Capacitance in F/g
1	3	315
2	6	291
3	9	268
4	12	251
5	15	232

Table 3: Cs from CV curves of Ni:Mn3O4electrodes at scan rate of 3mV/s.

S.No	Ni concentration in %	Specific Capacitance at scan rate of 3mV/s in F/g
1	0.0	315
2	0.3	384
3	0.6	421
4	0.9	396

Chrono potentiometric studies: Galvanostatic charge discharge (GCD) curves were hassled for the Mn_3O_4 and Ni:Mn_3O_4 electrodes as shown in figures 10, 11 and 12. Spinal structure of Mn_3O_4 with Mn^{2+} ions in tetrahedral sites and Mn^{3+} in octahedral sites [26] with a formula of $Mn^{2+}(Mn^{3+})_2O_4$ [30] give out high pseudocapacitance [31]. Specific capacitance was assessed from the formula, $C_s = \frac{I\,\Delta t}{m\,\Delta V}$, where I is current through the electrode, Δt is discharging time and ΔV is potential difference and m is active mass of the electrode. The figured specific capacitance for Mn_3O_4 electrodes were 264, 302, 352, 454 and 565 F/g at specific currents of 1.50, 1.25, 1.00, 0.75 and 0.50 A/g respectively. All these values are shown in table 3. For Ni:Mn_3O_4 electrodes at 0.0%, 0.3%, 0.6% and 0.9% Ni concentrations, the specific capacitance were 352, 426, 476 and 414 F/g respectively at a current density of 1A/g. These values were expose to view in table 4. The value of specific capacitance was maximum for 0.6% Ni doped Ni:Mn_3O_4 electrodes. The swing in these values also confirm the trends in the values drawn from CV curves. Finally, 0.6% Ni doped Mn_3O_4 electrodes were ply to study the GCD curves and its specific capacitance was found at specific currents of 1.50, 1.25, 1.00, 0.75 and 0.50A/g as 429, 448, 476, 529 and 626 F/g respectively. In the modus operandi, extortionate C_s cherished through hydrothermal course of action from Mn_3O_4 after doped with Ni.

S.No	Current density in A/g	Specific Capacitance in F/g
1	1.50	264
2	1.25	302
3	1.00	352
4	0.75	445
5	0.50	565

Table 4: C_s values of Mn_3O_4 electrodes form GCD curves.

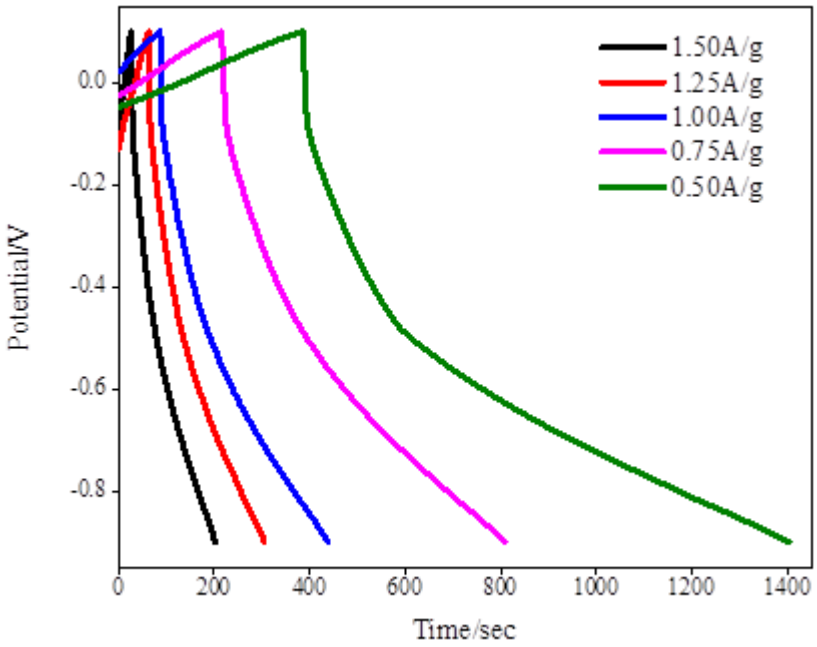

Fig. 10: CP curves of electrodes of Mn_3O_4 electrodes.

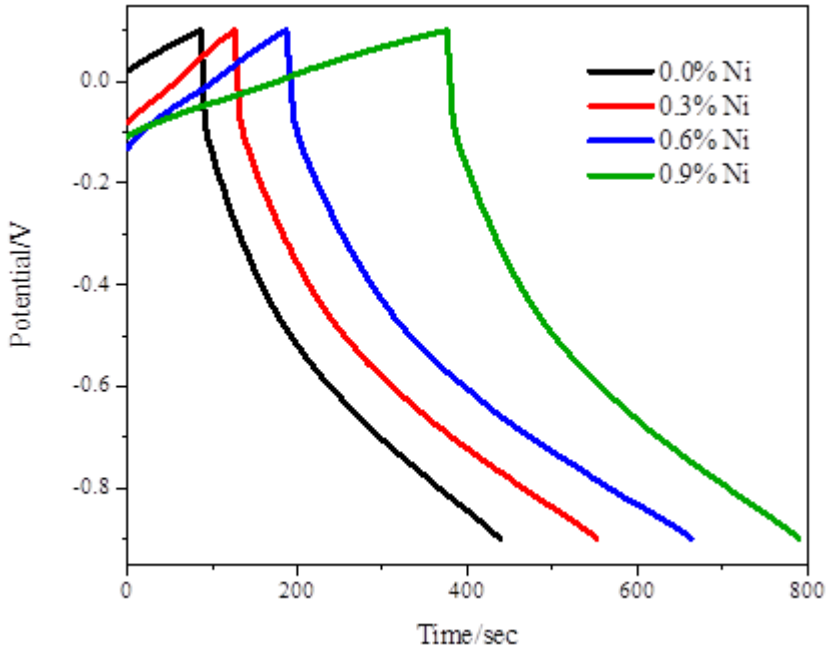

Fig. 11: CP curves of Ni:Mn_3O_4 electrodes.

S.No	% Ni concentration	Specific Capacitance at 1A/g in F/g
1	0.0 (Pure Mn_3O_4)	352
2	0.3	426
3	0.6	476
4	0.9	414

Table 5: C_s values of Ni:Mn_3O_4 electrodes form GCD curves.

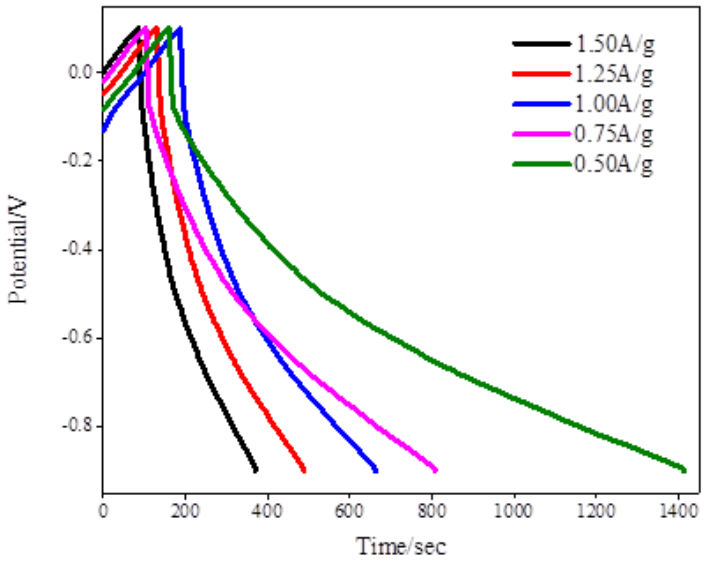

Fig. 12: CP curves of 0.6% Ni doped Mn_3O_4 electrodes.

Specific capacitance values from the aforementioned literature skimmed were observed and compared with the values obtained from the present work for the particles synthesized by hydrothermal method. Z. Liu et al synthesized hollow microcubes of Mn_3O_4 which have specific capacitance of 176 F/g at a specific current of 0.3 A/g [30]. Dadamiah P.M.D. Shaik et al synthesized octahedron shaped Mn_3O_4 octahedrons having specific capacitance of 198 F/g at 0.5mA/cm^2 [32]. H. Ullah Shah produce nanoparticles of Mn_3O_4 with a specific capacitance value 355 F/g at a specific current of 0.35 A/g [33]. Ultra fine nanoparticles of Mn3O4 exhibited a value of 401 F/g at a scan rate of 10mV/s [34]. Porous nanoparticles of Mn_3O_4 were produced by Dadamiah PMD Shaik exhibited specific capacitance value of 435 F/g at a scan rate of 1 mV/s [35]. All these utterances were shown in table 7 precisely.

S.No	Specific current in A/g	Specific Capacitance in F/g
1	1.50	429
2	1.25	448
3	1.00	476
4	0.75	529
5	0.50	626

Table 6: C_s values of 0.6%Ni:Mn_3O_4 electrodes form GCD curves.

Electrochemical Impedance Spectroscopic studies: To substantially confirm the capacitive nature and cyclic stability of the 0.6% Ni:Mn_3O_4 electrodes, EIS studies were accompanied on these electrodes. Ran through 3600 cycles, the solution resistance was increased from 12Ω to 27Ω, charge transfer resistance was decreased from 203Ω to 104Ω and the specific capacitance was found to be 82%. With the decrease of charge transfer resistance from 203 to 104 Ω, conductance increases in the same proportion, which leads to the curtailment of capacitance. It was also noticed in the decline of time period, when time period was set side by side between 1st cycle and 3600th cycle as shown in fig. 12. For these electrodes there was a low decrease of specific capacitance even after 3600 cycles.

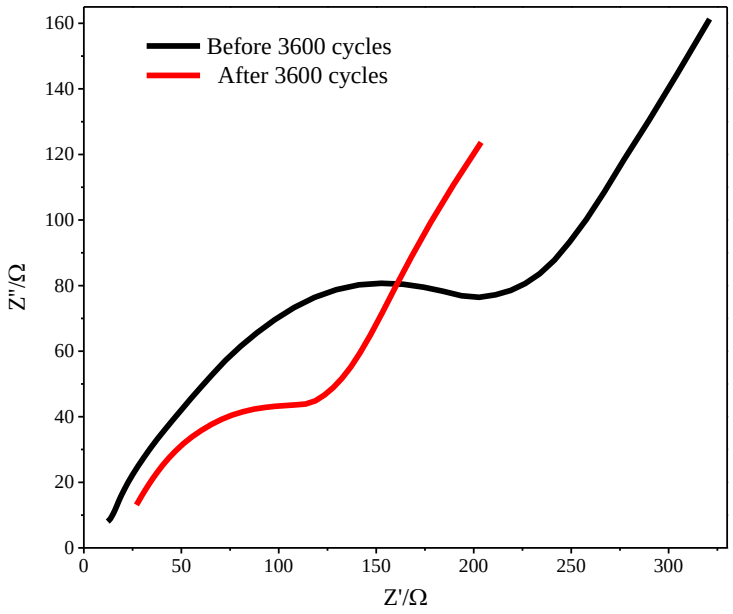

Fig. 13: Nyquist plots of 6% Ni doped Mn_3O_4 nanoparticles.

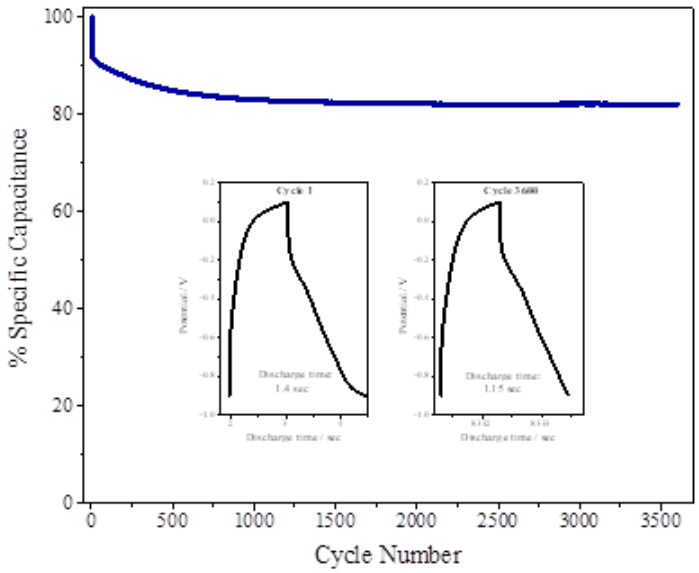

Fig. 14: Change of Specific Capacitance with cycle number.

V. Conclusion

Hydrothermal method of synthesis was followed for the preparations of Mn_3O_4, Ni:Mn_3O_4 nanoparticles. Crystalline structure was seasoned from XRD and Raman spectroscopic studies. At a reaction temperature 500K and reaction time of 15hours reliable yield resulted in the formation of decent crystalline nanoparticles of Ni:Mn_3O_4. Porous structure was rooted from morphology captured from scanning electron microscopy. Ni doped Mn_3O_4 nanoparticles with the doping concentration of 0.6% Ni exhibited better porous nature which is the key for super capacitors. Super capacitive properties of the Ni:Mn_3O_4 electrodes have shown a specific capacitance of 626 F/g at specific current of 0.50 A/g for 6% Ni concentration. These electrodes have exhibited a very good cyclic stability of 82% of the specific capacitance even after 3600 cycles. Finally, by hydrothermal method, maximum C_s value was successfully achieved from Mn_3O_4, by doping with Ni.

References

[1]. Hansa Mahajan, Joonho Bae, Kyusik Yun, Facile Synthesis Of Zno-Aunanocomposites For High-Performance Supercapacitors, J Alloys Comp 758 (2018) 131- 139.

[2]. Jiří Libich, Josef Máca, Jiří Vondrák, Ondřej Čech, Marie Sedlaříková, Supercapacitors: Properties And Applications, J. Energy Storage 17 (2018) 224–227.

[3]. G. Salazar-Alvarez, J.Sort, S. Surinach, M.D.B. Aro, J. Nogues, J. Am. Chem. Soc, 129, 9102-9108 (2007).

[4]. Y.-Z. Zhang, Y. Wang, T. Cheng, W.-Y. Lai, H. Pang, W. Huang, Flexible Supercapacitors Based On Paper Substrates: A New Paradigm For Low-Cost Energy Storage,Chem. Soc. Rev., 44 (2015) 5181-5199.

[5]. Jing Xu, Jiaqiang Li, Qiaoling Yang, Yan Xiong, Changguo Chen, In-Situ Synthesis Ofmno2@Graphdiyne Oxides Nanocomposite With Enhanced Performance Of Supercapacitors, Electrochem. Acta 251 (2017) 672-680.

[6]. Piaopiao Sun, Zhaohui Li, Lin Zhang, Cui Dong, Zhongjun Li, Hongchang Yao, Jianshe Wang, Guangheng Li, Synthesis Of Cobalt-Nickel Pyrophosphates/N-Doped Graphene Composites With High-Rate Capability For Asymmetric Supercapacitor, J Alloyscomp 750 (2018) 607-616.

[7]. M. Mondal, B. Das, P. Howli, N.S. Das, K.K. Chattopadhyay, Porosity-Tuned Nio Nanoflakes: Effect Of Calcination Temperature For High Performing Supercapacitor Application, J Electroanal Chem 813 (2018) 116-126.

[8]. Chao Feng, Liu Zachary G. Neale, Guozhong Cao, Understanding Electrochemical Potentials Of Cathode Materials In Rechargeable Batteries, Mater. Today 19 (2016) 109-123.

[9]. H. Chen, S. Zhou, M. Chen, L. Wu, Reduced Graphene Oxide–Mno2 Hollow Sphere Hybridnanostructures As High-Performance Electrochemical Capacitors, J. Mater. Chem., 22 (2012)25207-25216.

[10]. P. Yang, W. Mai, Flexible Solid-State Electrochemical Supercapacitors, Nano Energy, 8(2014) 274-290

[11]. Devadas A, Baranton S, Napporn T.W, Coutanceau C "Tailoring Of Ruo2 Nanoparticles By Microwave Assisted Instant Method For Energy Storage Applications" Journal Of Power Sources 196 (2011) 4044-4053.

[12]. Linrui Hou, Changzhou Yuan, Long Yang, Laifa Shen, Fang Zhang And Xiaogang Zhang " Urchin Like Co3o4 Micorspherical Hierarchical Superstructures Constructed By One Dimension Nanowires Towards Electrochemical Capacitors" Acs Advances 1 (2011) 1521-1526.

[13]. Han D, Xu P, Jing X, Wang J, Yang P, Shen Q, Liu J, Song D, Gao Z, Zhang M, J. Power Sources 235 (2013) 45-53.

[14]. Purushothan Reddy B, Sivajee Ganesh K, Jayanth Babu K, Hussain O.M, Julien. C M, Ionics 21 (2015) 2319-2328.

[15]. Wang B, Guan D, Gao Z, Wang J, Li Z, Yang W, Liu, Materials Chemistry And Physics 141(1) (2013) 1-8.

[16]. Weifengwei, Xinweicui, Weixing Chen, Douglas G. Ivey, Manganese Oxide-Based Materials As Electrochemical Supercapacitor Electrodes, Chem. Soc. Rev. 40 (2011) 1697–1721.

[17]. Fengliu Lou, Haitao Zhou, Fan Huang, Fride Vullum-Bruer, Trung Dung Tran, De Chen, Facile Synthesis Of Manganese Oxide/Aligned Carbon Nanotubes Over Aluminium Foil As 3d Binder Free Cathodes For Lithium-Ion Batteries, J. Mater. Chem. A 1 (2013) 3757-3767.

[18]. Mn_3o_4 Based Materials For Electrochemical Supercapacitors: Basic Principles, Charge Storage Mechanism, Progress, And Perspectives Author Links Open Overlay Panel S.A. Beknalkar [A], A.M. Teli [B], T.S. Bhat [A C], K.K. Pawar [A C], S.S. Patil [A], N.S. Harale [D], J.C. Shin [B], P.S. Patil [A C] Https://Doi.Org/10.1016/J.Jmst.2022.03.036

[19]. Dadamiah P.M.D. Shaik, P. Rosaiah, O.M. Hussain, Supercapacitive Performance Ofmn3o4 Nanoparticles Synthesized By Hydrothermal Method, Adv. Sci. Eng. Med. 8(2016) 1–6.

[20]. P. Rosaiah, Jinghui Zhu, O.M. Hussain, Yejun Qiu, Synthesis Of Flower Like Reduced Graphene Oxide-Mn3o4 Nanocomposite Electrodes For Supercapacitors, Appl. Phys. A124 (2018) 1–9.

[21]. Fabrication Of The Mn3o4 Thin Film Electrodes By Electron Beam Evaporation For Supercapacitor Applications. Dadamiah P.M.D. Shaik, P. Rosaiah, O.M. Hussain, Https://Doi.Org/10.1016/J.Elechem.2019.113409

[22]. Hong-Yan Wang, Deng-Gong Li, Hui-Ling Zhu,Yong-Xin Qi, Hui Li, Ning Lun, Yu-Jun Bai, Mn3o4/Ni(Oh)2 Nanocompositeas An Applicable Electrode Material For Pseudocapacitors, Electrochimicaacta Http://Dx.Doi.Org/10.1016/J.Electacta.2017.08.015

[23]. B. Wang, Q. Liu, Z. Qian, X. Zhang, J. Wang, Z. Li, H. Yan, Z. Gao, F. Zhao, L. Liu,Two Steps In Situ Structure Fabrication Of Ni–Al Layered Double Hydroxide On Ni Foam And Its Electrochemical Performance For Supercapacitors, J. Power Sources., 246 (2014) 747-753.

[24]. G.M. Biggar, Short Communications Mineralogical Magazine 37 (1969) 286-287.

[25]. T. Ozkaya, A. Baykal, H. Kavas, Y. Koseoglu, M.S. Toprak, A Novel Synthetic Route To Mn3o4 Nanoparticles And Their Magnetic Evaluation, Phys. B 403 (2008) 3760–3764.

[26]. D. P. Dubal , D. S. Dhawale , R. R. Salunkhe , S. M. Pawar And C. D. Lokhande , Appl. Surf. Sci., 2010, 256 , 4411 —4416.

[27]. J. S. Hong, H. Seo, Y. H. Lee, K. H. Cho, C. Ko, Dr. S. Park, Prof. K. T. Nam, Doi: 10.1002/Smtd.201900733

[28]. Chen, Elizabeth R. (2008). "A Dense Packing Of Regular Tetrahedra". Discrete & Computational Geometry. 40(2):214-240. Doi:10.1038/460801a

[29]. Cohn, Henry (2009). Mathematical Physics: A Tight Squeeze". Nature. 460 (7257):801-802. Bicode:2009nature.460..801c.

[30]. Phansirisuktha, Nutthaphonphattharasupakun, Peerapandittanet And Montreesawangphruk, Charge Storage Mechanisms Of Electrospun Mn3o4 Nanofibres For High-Performance Supercapacitors.Https://Doi.Org/10.1039/C6ra28499j

[31]. Z. Liu, Li Zhang, G. Xu, L. Zhang, D. Jia, C. Zhang, Mn3o4 Hollow Microcubes And Solid Nanospheres Derived From A Metal Formate Framework For Electrochemical Capacitor Applications, Rsc Adv. 7 (2017) 11129–11134.

[32]. H. Ullah Shah, F. Wang, A. Mohammad Toufiq, A. Muqsit Khattak, Azhar Iqbal, Zahid Ali Ghazi, Shujaat Ali, X. Li, Ziya Wang, Electrochemical Properties Of Singlecrystalline Mn3o4 Nanostructures And Their Capacitive Performance In Basic Electrolyte, Int. J. Electrochem. Sci. 11 (2016) 8155–8162.
[33]. L. Laffont And P. Gibot , Mater. Charact., 2010, 61 , 1268 —1273.
[34]. Enhanced Supercapacitive Performance Of Nanocrystalline Mn3o4 Synthesized By Hydrothermal Method.Dadamiah Pmd Shaika, P. Rosaiahb And O M Hussain, Council For Innovative Research, Journal Of Advances In Chemistry, Vol. 12, No. 1, Page 3919, N O V E M B E R 1 1 , 2 0 1 5.
[35]. Dadamiah P.M.D. Shaik, P. Rosaiah, O.M. Hussain, Supercapacitive Properties Of Mn3o4 Nanoparticles Synthesized By Hydrothermal Method, Mater. Today Proc. 3 (2016) 64–73.